Steel and Composite Structures, *Vol. 43, No. 3 (2022) 000-000*
https://doi.org/10.12989/scs.2022.43.3.000

Modeling of composite MRFs with CFT columns and WF beams

Ricardo A. Herrera[1a], Teerawut Muhummud[2a], James M. Ricles*[3] and Richard Sause[3b]

[1]*Dept of Civil Engineering, University of Chile, Av. Blanco Encalada 2002, Piso 4, 8370449 Santiago, Chile*
[2]*Dept of Civil Technology Education, King Mongkut's University of Technology Thonburi, 91 Pracha-U-thit Road, Bangmod, Thungkru, Bangkok, Thailand*
[3]*Dept. of Civil and Environmental Engineering, Lehigh Univ., 117 ATLSS Dr., Bethlehem, PA 18015, USA*

(Received March 15, 2022, Revised April 16, 2022, Accepted April 16, 2022)

Abstract. A vast amount of experimental and analytical research has been conducted related to the seismic behavior and performance of concrete filled steel tubular (CFT) columns. This research has resulted in a wealth of information on the component behavior. However, analytical and experimental data for structural systems with CFT columns is limited, and the well-known behavior of steel or concrete structures is assumed valid for designing these systems. This paper presents the development of an analytical model for nonlinear analysis of composite moment resisting frame (CFT-MRF) systems with CFT columns and steel wide-flange (WF) beams under seismic loading. The model integrates component models for steel WF beams, CFT columns, connections between CFT columns and WF beams, and CFT panel zones. These component models account for nonlinear behavior due to steel yielding and local buckling in the beams and columns, concrete cracking and crushing in the columns, and yielding of panel zones and connections. Component tests were used to validate the component models. The model for a CFT-MRF considers second order geometric effects from the gravity load bearing system using a lean-on column. The experimental results from the testing of a four-story CFT-MRF test structure are used as a benchmark to validate the modeling procedure. An analytical model of the test structure was created using the modeling procedure and imposed-displacement analyses were used to reproduce the tests with the analytical model of the test structure. Good agreement was found at the global and local level. The model reproduced reasonably well the story shear-story drift response as well as the column, beam and connection moment-rotation response, but overpredicted the inelastic deformation of the panel zone.

Keywords: analytical models; composite moment resisting frames; concrete filled tube columns; earthquake resistant structures; high strength concretel; high strength steel; nonlinear analysis; steel wide flange beams

1. Introduction

Concrete and steel composite construction combines the structural and economic advantages of both materials, including the speed of construction, strength, long-span capability, and light weight of structural steel, and the inherent mass, stiffness, damping, and cost economy of reinforced concrete. Due to these advantages, composite structural systems, including moment resisting frames (MRFs) and braced frames, where some or all the elements are composite, have been used to resist gravity, wind, and seismic loading. A concrete filled tube moment resisting frame (CFT-MRF) is one type of composite MRF system where concrete-filled steel tubular (CFT) columns are used in conjunction with steel wide-flange (WF) beams. The steel tube of a CFT serves as formwork and offers confinement to the concrete, while the concrete infill delays the development of local buckling of the steel tube.

A significant amount of research has been conducted to develop analysis tools and design guidelines for CFT-MRFs under seismic loading. Several experimental studies, discussed below, have been conducted on the behavior of CFT-MRF components, namely CFT columns, WF beams, connections, and panel zones.

1.1 CFT Column Modeling

Several discrete element formulations have been developed to model CFT columns in large sub-assemblages, including: a fiber-based element by Inai and Sakino (1996) where the fiber stress-strain relationships are determined based on empirical equations calibrated to the results from an extensive CFT column testing program by Fujimoto *et al*. (1996) a three-dimensional distributed plasticity element formulation for CFT beam-column members by Hajjar *et al*. (1998a) calibrated using the results of CFT flexural tests conducted by Tomii and Sakino (1979) and, a fiber based model by Varma *et al*. (2005) which uses effective uniaxial stress-strain curves for the steel and concrete fibers obtained from finite element analysis of the failure region of a CFT column calibrated to tests results (Varma *et al*. 2002, 2004). According to Zhang and Shahrooz (1997), Inai and Sakino's model (1996) is too conservative for CFT columns made of conventional materials. Hajjar *et al*. (1998a) note that their formulation does not account explicitly for local buckling and biaxial stress conditions in the steel tube, despite accounting for geometric and material nonlinearities

*Corresponding author, P.E., Ph.D. Professor
E-mail: jmr5@lehigh.edu
[a]Ph.D. Associate Professor
[b]Ph.D. Professor

ISSN: 1229-9367 (Print), 1598-6233 (Online)

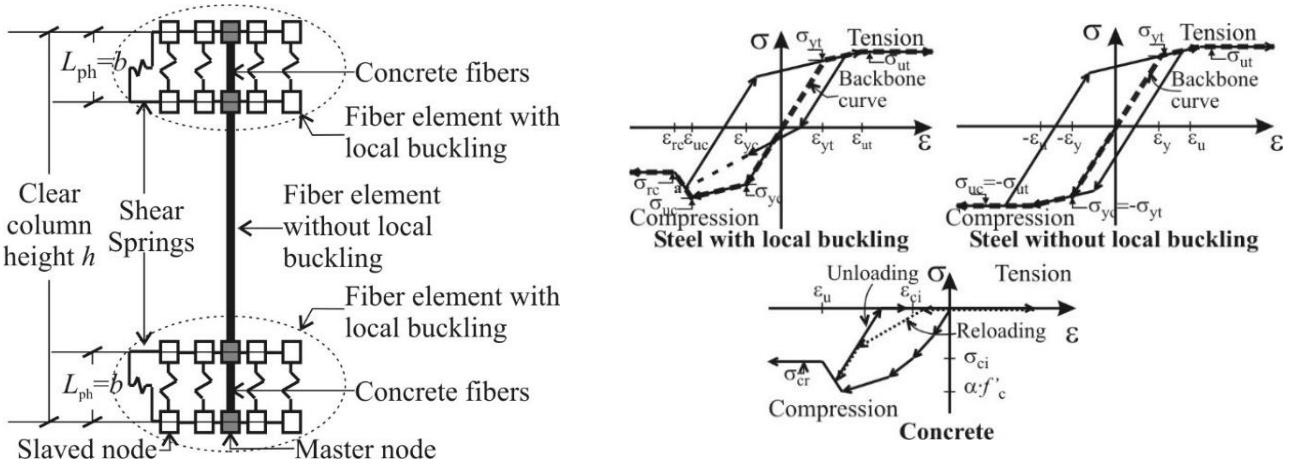

(a) Complete CFT column model (b) Effective fiber stress-strain curves

Fig. 1 Analytical model of CFT column

including slip between the steel and concrete surfaces, steel yielding, concrete strength and stiffness degradation, and the effect of confinement and cyclic loading on the concrete core. Consequently, good correlation with experimental results is found only up to the onset of local buckling. The model by Varma *et al*. (2005), on the other hand, implicitly accounts for the effects of local buckling and biaxial stress conditions in the steel tube, in addition to the other effects considered in the model of Hajjar *et al*. (1998a).

1.2 Connection Modeling

An integrated experimental and analytical research program conducted by Peng *et al*. (2001) and Ricles *et al*. (2004) tested several different WF beam-to-CFT column connections, including interior diaphragm, bolted split-tee, and welded split-tee connections. These studies concluded that the best performance was achieved by the welded split-tee connection, where the tee stem is welded to the beam flange and the tee flange is bolted to the CFT column by passing high-strength unbonded rods through the column. As part of the study by Peng *et al*. (2001), a multi-component model to account for the elastic stiffness of split-tee connections was developed based on a model by Swanson and Leon (2001) for bolted split-tee steel WF beam-to-WF column connections. The model considered the contributions of the tee flange deformation, tension bolt elongation, tee stem elongation, and column panel zone bearing deformation to the connection flexibility.

1.3 Panel Zone Modeling

Kanatani *et al*. (1987) developed a CFT column panel zone model with split-tee bolted connections using a strut-and-tie based model. The model was based on the formation of an inclined compressive strut in the concrete infill of the joint under shear force. Koester (2000) conducted research on CFT column panel zones with welded split-tee connections bolted to a CFT column. Based on the test results, Koester proposed that the shear capacity V_u of the CFT column panel zone consisted of contributions by the steel tube and the concrete infill.

1.4 Composite Structural System Modeling

Only a few models for entire composite structural systems have been developed. Integrating the distributed plasticity model for the CFT column they had developed, Hajjar *et al*. (1998b) created a model of a four-story composite frame and analyzed it under a combination of gravity and wind loads. The analysis results showed that slip between the steel and concrete surfaces had little effect on the global behavior of a composite CFT frame and on the strength of a CFT member subjected to flexure. Mehanny and Deierlein (2001) developed a model of a composite frame with reinforced concrete columns and steel beams using fiber elements and used it to perform nonlinear time-history analysis and evaluate the performance of the frame when subjected to increasing levels of seismic excitation. The composite frame was not a CFT-MRF.

Models for CFT-MRFs are needed which have been calibrated against large-scale tests of CFT-MRFs and consider the important limit states that can occur in the members and components of the system under seismic loading conditions. This paper presents the results of research related to the development and calibration of an analytical model for the seismic response of CFT-MRFs. The model of the system is comprised of models of the components of a CFT-MRF, including the CFT columns, WF beams, beam-to-column connection elements, and the CFT panel zones. The model considers the limit states mentioned above in the CFTs, WF beams, connection elements, and CFT panel zone. The model of each component is validated from experimental data, and the CFT-MRF model used to analyze a large-scale SC-MRF tested by Herrera *et al*. (2008). The behavior predicted by the model of the CFT-MRF is compared to the test results, which included the elastic modal periods and inelastic response under the design basis earthquake, DBE, and maximum considered earthquake, MCE. In accordance with FEMA (2003), which is the criteria used to design the test structure, the MCE has a probability of occurrence of 2% in

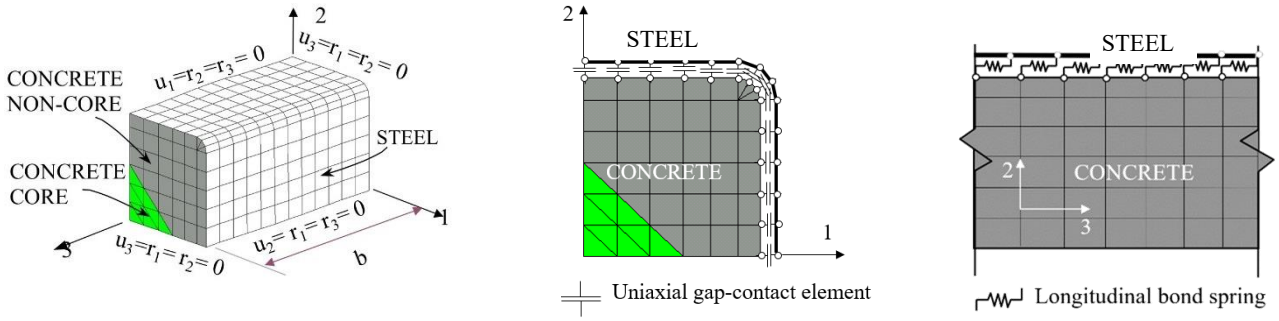

(a) Overall view (b) Transverse interaction (c) Longitudinal interaction

Fig. 2 Finite element model for failure segment of CFT column (Varma *et al*. 2005)

Table 1 Concrete effective stress-strain data for SR6C4C specimen model

ε (mm/mm)	σ (MPa)
0.00093	25.1
0.00203	43.7
0.00316 (= ε_{ci})	51.8 (= σ_{ci})
0.00584	54.5 (= $\alpha f'_c$)
0.07500 (= ε_u)	31.0 (= σ_{cr})

Table 2 Steel effective stress-strain data for SR6C4C specimen model

σ_{yt} (MPa)	540
ε_{yt} (mm/mm)	0.0027
σ_{ut} (MPa)	545.4
ε_{ut} (mm/mm)	0.124
σ_{yc} (MPa)	493.6
ε_{yc} (mm/mm)	0.0025
σ_{uc} (MPa)	493.6
ε_{uc} (mm/mm)	0.0029
σ_{rc} (MPa)	450
ε_{rc} (mm/mm)	0.0049

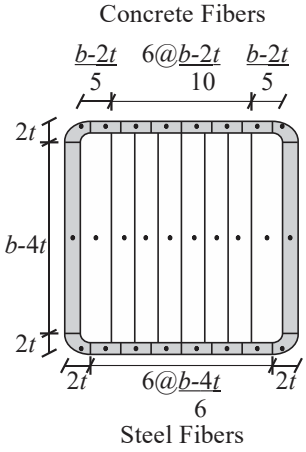

Fig. 3 SR6C4C specimen cross section discretization

50 years while the DBE has an intensity equal to two-thirds that of the MCE.

2. Modeling of CFT-MRF components

2.1 CFT Column Model

Because of its ability to capture the local buckling of the steel tube, the fiber-based model developed and calibrated by Varma *et al*. (2005) is used as the basis for the model of the column behavior in the plastic hinge region (i.e., at the ends of the column that are of length L_{ph}), where steel local buckling and concrete crushing may occur and cause strength degradation in a column. Outside of this region, a fiber element with no consideration for local buckling of the steel is used. The general column model is shown in Fig. 1, as well as effective stress-strain curves representing the stress-strain behavior of steel and concrete in each region of a CFT column. The concrete fibers are assumed to have zero tensile strength. The steel fibers outside the plastic hinge region are modeled using identical elastic-plastic with kinematic hardening relationships in tension and compression, where the yield, σ_y, and ultimate stress, σ_u, and the corresponding respective strain values ε_y and ε_u are obtained from tensile coupon tests. This same curve is used in tension for the steel fibers in the plastic hinge region, while a region of decreasing strength with increasing deformation is included in compression to account for the strength degradation after local buckling of the steel tube occurs, as shown in Fig. 1(b). A kinematic hardening rule is followed in compression until the buckling stress is reached. Following the onset of local buckling, a degradation of the compression stiffness in the stress-strain curves under cyclic loading is modeled by reloading to the previous maximum deformation reached on the compression side, as shown in Fig. 1(b). The compressive backbone stress-strain curves for steel and concrete fibers in the plastic hinge zone (termed "effective stress-strain" curves) are determined using the nonlinear finite element model (FEM), shown in Fig. 2, developed by Varma *et al*. (2005), to account for concrete crushing and cracking, steel yielding and local buckling, and bond slip between the steel and concrete of the CFT. The model shown in Fig. 2(a) considers the symmetry of the CFT cross section, enabling the model to be developed consisting of one-quarter the cross-section. The effective stress-strain curves are determined by considering the average stress in the concrete and the steel (load divided by cross-sectional area) and strain (shortening divided by original length) in the FEM. The length of the plastic hinge region (L_{ph}) is assumed to be equal to the column depth b, based on recommendations

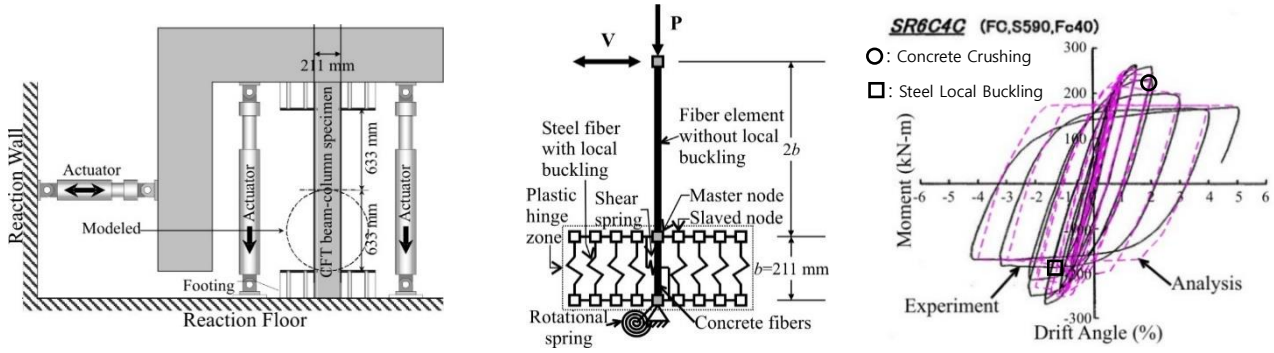

(a) Test setup (b) Analytical model (c) Comparison of results

Fig. 4 Validation of analytical CFT column model for specimen SR6C4C (Fujimoto *et al*. 1996)

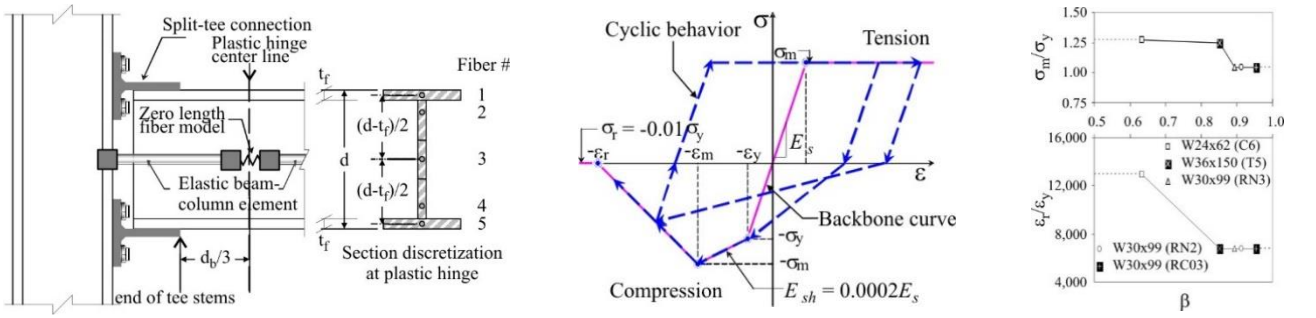

(a) Model of WF beam in MRF (b) Fiber stress-strain relationship for plastic hinge (c) Stress-strain curve parameters

Fig. 5 Analytical model of WF beam

from Varma *et al*. (2005).

The model for CFT columns was validated using test data of Specimen SR6C4C from Fujimoto *et al*. (1996). The specimen has a tube width-to-thickness, b/t, ratio of 35.5, a steel tube yield stress σ_y equal to 609 MPa, and concrete infill compressive stress f'$_c$ equal to 39.1 MPa. The properties and geometry of this specimen were the closest available to the CFT columns of the CFT-MRF of Herrera *et al*. (2008) that was to be modeled. The data for the effective stress-strain curves for the concrete and steel are given in Tables 1-2.

The discretization of the CFT cross-section for the fiber model is shown in Fig. 3, consisting of 8 fibers for the concrete and 10 fibers for the steel tube. The test specimen was subjected to a constant axial load P of 40% of its axial load capacity of N_0 = 4315 kN, while undergoing cycles of increasing drift up to about 5% rads.

Analytical and experimental column responses compared favorably as shown in Fig. 4. The strength degradation in the test specimen following steel local buckling and concrete crushing is captured by the model. The results in Fig. 3 indicate that the model can be used to predict the response of CFT columns which develop inelastic response that include local steel buckling and concrete crushing.

2.2 WF Beam Model

The fiber-based model developed by Muhummud (2004) shown in Fig. 5 was used to model the WF beam plastic hinge region behavior under cyclic loading conditions. A zero-length fiber element is used for the model, where the inelastic behavior of the beam is concentrated at the center of the beam plastic hinge location and the cross section is discretized as shown in Fig. 5(a) using 5 fibers. The fibers are symmetrically positioned with respect to the beam centerline, at a distance such that the resulting plastic section modulus Z is equal to the nominal value given in the AISC Steel Construction Manual (AISC 2017).

Table 3 Beam properties from tests used for beam model calibration studies

Specimen - source	Beam section	Steel grade	σ_y (MPa)
C6 - Peng *et al*. (2001)	W24x62	A36	248
T5 - Ricles *et al*. (2002)	W36x150	A992, Gr. 50	345
RN2 - SAC (1997)	W30x99	A36	248
RN3 - SAC (1997)	W30x99	A36	248
RC03 - Kim *et al*. (2000)	W30x99	A992, Gr. 50	345

The model can capture the strength degradation in the beam after the onset of local buckling by implicitly accounting for the effects of steel local buckling in the effective stress-strain curves of the steel fibers. The cyclic stress-strain relationship for the steel in the beam model, illustrated in Fig. 5(b), is defined by four parameters, namely yield stress σ_y, elastic modulus of steel E_s, maximum stress σ_m, and residual strain ε_r. The latter corresponds to the strain at which the fiber has lost most of its strength (assumed to be equal to $0.01\sigma_y$) after extensive

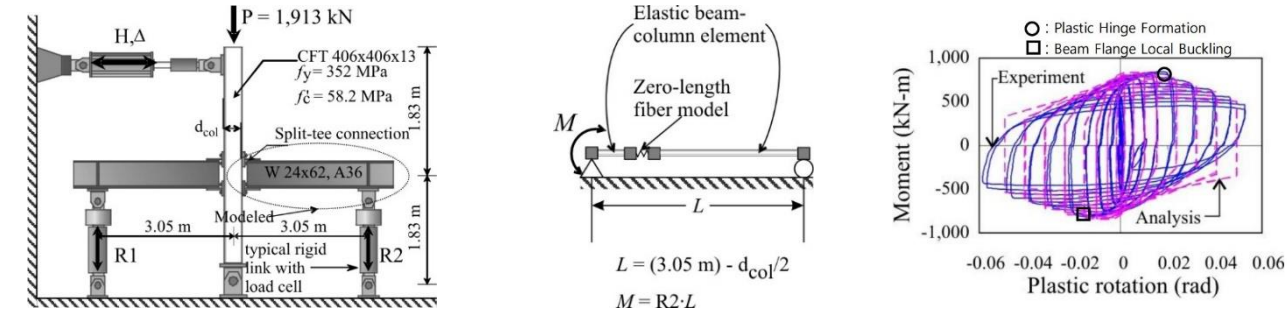

(a) Test setup schematic (b) Analytical model (c) Comparison of results

Fig. 6 Calibration of WF beam analytical model for specimen C6 (Peng *et al*. 2001)

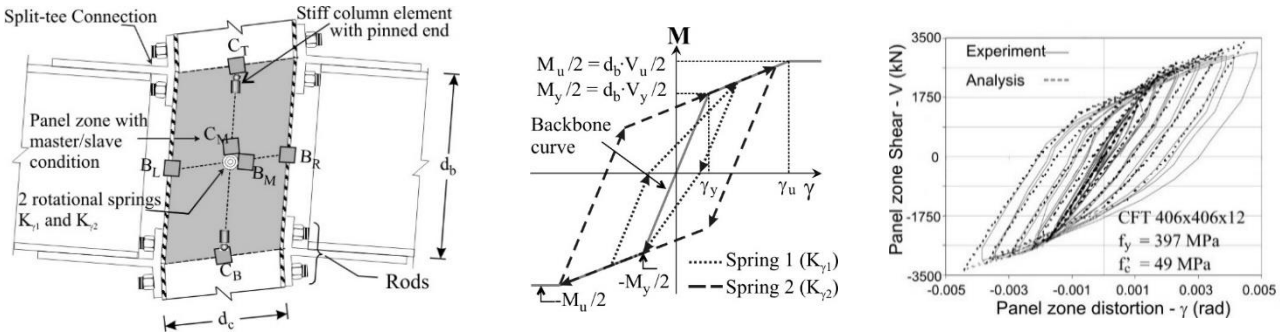

(a) Model of CFT panel zone in MRF (b) Springs cyclic response (c) Model calibration

Fig. 7 Analytical model of CFT panel zone (calibration by Muhummud 2004)

local buckling develops.

The values of σ_y and E_s are determined from tensile coupon tests, while the values of σ_m and ε_r are obtained from empirical curves that were calibrated using results from five beam tests with inelastic cyclic loading. Table 3 lists the specimen identification and beam properties for each test.

Fig. 5(c) shows the values of σ_m and ε_r from the calibration studies and the resulting curves as a function of β, a normalized slenderness ratio defined by Eq. (1).

$$\beta = \sqrt{(\beta_f^2 + \beta_w^2)/2} \tag{1}$$

In Eq. (1) β_f and β_w are normalized width-to-thickness ratios for the beam flange and web, respectively, calculated according to Eq. (2), where b/2t and h/t_w are the width-to-thickness ratios of the WF beam flange and web, respectively. The denominators in Eq. (2) are the limiting width-to-thickness ratios for members with a compactness (λ_p) specified in the AISC Seismic Provisions (AISC 2005) for flanges and webs in flexural compression, respectively.

$$\beta_f = \frac{b/2t}{52/\sqrt{\sigma_{yf}}}\ ,\ \beta_w = \frac{h/t_w}{520/\sqrt{\sigma_{yw}}} \tag{2}$$

The quantities σ_{yf} and σ_{yw} in Eq. (2) are the measured yield stress of the flanges and the web, respectively. The 2005 AISC Seismic Specification compactness limits are used to develop Eq. (2), for it was the current specification at the time of the research by Herrera *et al*. (2008).

The transverse shear behavior across the plastic hinge is assumed to be elastic and elastic beam elements are used to model other portions of the beam outside of the plastic hinge region.

Figs. 6(a) and 6(b) show the test setup and analytical model of Specimen C6. The test subassembly was subjected to cycles of increasing drift up to about 7% rads. Fig. 6(c) shows the hysteretic response of the moment-plastic rotation in the plastic hinge region of the beam. The test specimen during the experiment developed a plastic hinge at the first excursion to a plastic rotation of about 2% rads. During the second subsequent cycle to this plastic rotation local flange buckling occurred, which was almost immediately proceeded by local web buckling in the beam plastic hinge region. Subsequently cycles of drift applied to the test specimen led to extensive cyclic local buckling and a deterioration in flexural capacity of the beam, as shown in Fig. 6(c). The model used in the analysis was able to capture the plasticity and local buckling that occurred in the test specimen. This is evident by the good comparison between the experimental results with the model predictions for Specimen C6 in Fig. 6(c). These comparisons represent typical results between experimental and model predictions for all the specimens in Table 3.

2.3 Panel Zone Model

The CFT column panel zone was modeled using a kinematics-based model, shown in Fig. 7(a) in its deformed configuration. The model was calibrated to the experimental data of Koester (2000). In the model, nodes CM and BM have the same coordinates and translational degrees of freedom (DOFs), while having independent rotations. Nodes CM and BM are connected by a pair of parallel

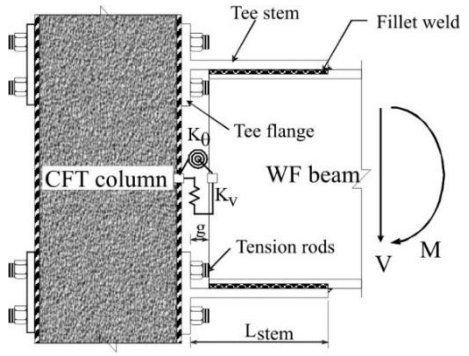

(a) Connection model

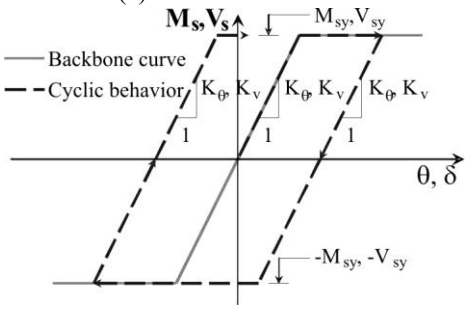

(b) Spring properties

Fig. 8 Analytical model of split-tee connection (Peng *et al*. 2001)

rotational spring elements representing the shear flexibility of the panel zone. At the column faces, the translational DOFs of nodes BL and BR are slaved to node BM, while the rotational DOFs of these nodes are slaved to node CM. At the top and bottom of the panel zone, the translational DOFs of nodes CT and CB are slaved to node CM and the rotational DOFs to node BM.

The effects of concrete cracking, concrete crushing, and steel yielding are considered in the panel zone shear force-shear deformation (V-γ) relationship. The effect of steel tube local buckling is not modeled because panel zone strength degradation was not observed in the tests conducted by Koester (2000). The parameters defining the backbone V-γ relationship for the CFT panel zone are: the elastic stiffness ($K_{\gamma,e}$); the panel zone shear at the onset of inelastic behavior (V_y); the inelastic stiffness ($K_{\gamma,i}$); and the panel zone shear capacity (V_u). The elastic stiffness $K_{\gamma,e}$ is calculated as the sum of the shear stiffnesses of the steel tube and concrete infill. The area of the concrete infill considered when determining $K_{\gamma,e}$ is the gross area of the concrete infill. The panel zone capacity V_u in kN is determined using Eq. (3):

$$V_u = V_s + V_c = \left(A_{web}\sigma_y/\sqrt{3} + 337.2A_c\sqrt{f_c'}\right)/1000 \quad (3)$$

In Eq. (3) A_{web}, σ_y, A_c, and f_c' are equal to area of the web of the steel tube (mm2), the yield stress of the steel tube (MPa), the area of the concrete core within the CFT column panel zone (mm2), and the compressive strength of the concrete infill (MPa), respectively.

Calibration studies conducted by Muhummud (2004) yielded values of V_y and $K_{\gamma,i}$ of $0.6V_u$ and $0.2K_{\gamma,e}$, respectively. The associated moment-rotation (M-θ) relationship of each rotational spring, $K_{\gamma1}$ and $K_{\gamma2}$, is obtained from the shear-deformation (V-γ) relationship of the CFT panel zone by taking M = 0.5V·d, and θ = γ.

Table 4 Combined elastic stiffness K_{bfb} of split-tee contributed by tension bolts, tee flange, and bearing deformation in CFT column (Peng *et al*. 2001)

CFT column b/t	Tee flange thickness (mm)	K_{bfb} (kN/mm)
32	12.7	772.3
	27.4	4640.9
48	12.7	753.0
	27.4	4553.3

The two parallel rotational springs, spring 1 (i.e., $K_{\gamma1}$) and spring 2 (i.e., $K_{\gamma2}$), differ only on the reloading behavior. The former reloads from zero to the point of previous maximum displacement, while spring 2 exhibits kinematic hardening until it reaches its maximum capacity (see Fig. 7(b)); after that the reloading path is similar to that of spring 1. This configuration showed the best correlation in the calibration studies by Muhummud (2004), as illustrated in Fig. 7(c) for one of the panel zone specimens tested by Koester (2000).

2.4 Connection Model

Based on research by Peng *et al*. (2001) and Ricles *et al*. (2004), the welded split-tee connection shown in Fig. 8(a) was used in the design of the CFT-MRF tested by Herrera *et al*. (2008). The split-tee connection is modeled using zero-length equivalent rotational and vertical elastic-plastic springs, labeled as K_θ and K_v, respectively, in Fig. 8(a).

The cyclic behavior of the rotational and transverse spring elements is shown in Fig. 8(b). The determination of K_θ, K_v, M_{sy}, and V_{sy} for these spring elements is discussed below.

The elastic stiffness of the rotational spring is based on the multi-component model developed by Peng *et al*. (2001). The stiffness of the tee in compression is defined by the connection stiffness contributed by the tee stem axial stiffness K_{stem}. For the tee in tension, the column panel zone bearing stiffness $K_{bearing}$, tension bolt stiffness K_{bolt}, tee flange stiffness K_{flange}, and tee stem stiffness K_{stem} all contribute to the connection elastic stiffness. The stiffnesses $K_{bearing}$, K_{flange}, and K_{bolt} are combined as K_{bfb} and determined from a finite element analysis because their inherently coupled behavior cannot be separated conveniently into individual springs. The values of K_{bfb} determined by Peng *et al*. (2001) are listed in Table 4. For b/t ratios not listed in Table 4, Peng *et al*. (2001) recommended performing additional finite element analysis for the desired configuration. For smaller b/t ratios, a conservative estimate of the connection deformation can be obtained using the values for a b/t of 32.

The elastic stiffness of the rotational spring element (K_θ) is then determined by combining the stiffnesses of the tees in tension and compression using Eq. (4).

$$K_\theta = \frac{{d_b}^2}{\left({K_{bfb}}^{-1} + {K_{stem}}^{-1}\right)^{-1} + {K_{stem}}^{-1}} \quad (4)$$

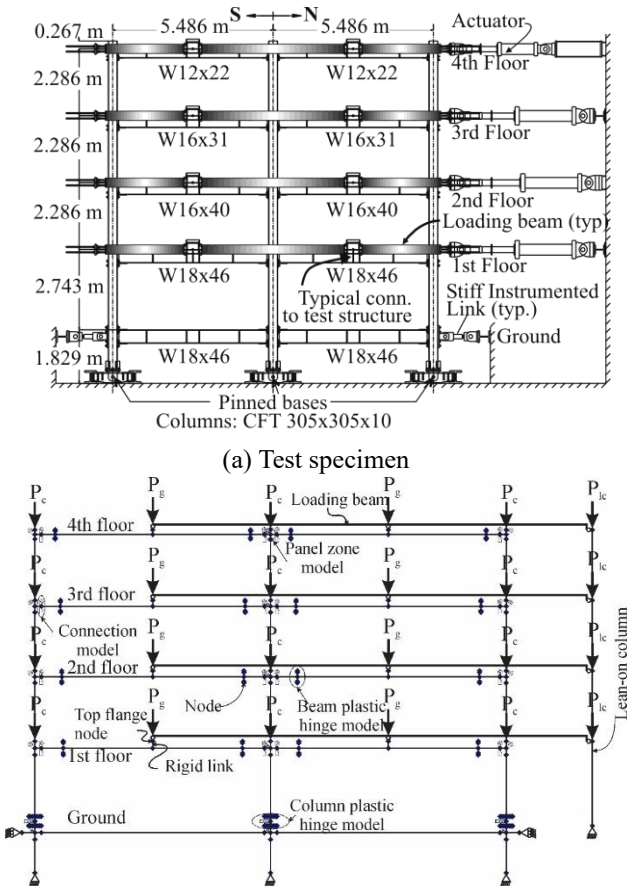

Fig. 9 Schematic and model of CFT-MRF tested by Herrera *et al*. (2008)

In Eq. (4) d_b is the beam depth and $K_{stem} = E_s \cdot A_{stem}/g$, where E_s is the modulus of elasticity of the steel, A_{stem} is the cross-sectional area of the tee stem, and g is the distance between the face of the tee flange and the beam end (see Fig. 8(a)).

The capacity of the rotational spring element (M_{sy} in Fig. 8(b)) is equal to the connection flexural capacity, calculated as the product of the tee stem axial capacity (tee stem cross-sectional area times its yield strength) and the depth between centerlines of the tee stems.

The transverse stiffness of the connection (K_v) is determined by modeling the tee stems as cantilever members subjected to the beam shear force, resulting in Eq. (5):

$$K_v = \frac{2}{\frac{g^3}{3E_s I_{stem}} + \frac{g}{G_s\left(\frac{5}{6}A_{stem}\right)}} \quad (5)$$

In Eq. (5), g and A_{stem} were previously defined, I_{stem} is the moment of inertia of one tee stem, and G_s is the shear modulus of elasticity of the steel.

The transverse shear capacity of the connection (V_{sy}) in Fig. 8(b) is the minimum between the tee flange-CFT column interface frictional capacity and the shear capacity of the tee stem, the latter calculated using the von Mises yield criterion.

Table 5 Concrete fiber parameters for the test frame CFT column model

ε (mm/mm)	σ (MPa)
0.00129	40.5
0.00220	60.0
0.00298 (= ε_{ci})	67.7 (= σ_{ci})
0.00439	70.0 (= $\alpha f'_c$)
0.02500(= ε_u)	51.7 (= σ_{cr})

3. Verification study

3.1 Description of test structure and model

The four-story CFT-MRF tested by Herrera *et al*. (2008), shown in Fig. 9(a), was modeled by using the procedure described above to model each component of the structure. The computer program DRAIN-2DX (Prakash *et al*. 1993) was used, which has a library of elements (e.g., displacement-based fiber elements to model the WF beams and CFT columns; rotational and translation spring elements to model the panel zones and connection components) and materials (concrete, steel). The test was performed using the hybrid simulation test method (Herrera *et al*., 2008), where several tests were performed at different seismic hazard levels. These hazard levels include the frequently occurring earthquake (FOE), the design basis earthquake (DBE), and the maximum considered earthquake (MCE). The FOE has a 50% probability of exceedance in 50 years, while the MCE has a probability of exceedance of 2% in 50 years, and the DBE an intensity that is 2/3rd that of the MCE (FEMA 2003).

The CFT columns of the test structure consisted of 305x305x10 mm A500 Grade 80 steel tubes filled with 55 MPa nominal strength concrete. The wide flange beams were A992 Grade 50 steel that ranged in size from W12 × 22 to W18 × 46, as shown in Fig. 9(a). The member sizes and material properties from material tests can be found in Herrera *et al*. (2008). The concrete compressive strength f'_c over the course of the frame testing was monitored using concrete cylinder material tests, where the average compressive strength was 67.6 MPa.

In the hybrid simulations, the displacements were imposed to each floor of the test frame using servo-hydraulic controlled actuators and stiff loading beams placed at each floor that simulated the floor diaphragm lateral force collector system (see Fig. 9(a)). The loading beams were connected to the WF beams of the test structure at midspan of both bays at each floor level. The effect of the interior gravity frames was included in the test through hybrid simulation.

The model of the test structure, shown in Fig. 9(b), included the local buckling of the steel tube at the base of the first story columns. A fiber element with no local buckling modeling capabilities was used for the remaining length of the first story columns and the columns in the other stories where local buckling in the steel tube is not expected to occur. The effective stress-strain curves in compression for the steel and the concrete in the plastic hinge region were generated using the finite element model

Table 6 Steel fiber parameters for the test frame CFT column model

Part	σ_{yt} (MPa)	σ_{ut} (MPa)	σ_{yc} (MPa)	σ_{uc} (MPa)	σ_{rc} (MPa)	ε_{ut}	ε_{uc}	ε_{rc}
Walls	601.6	607.6	547.7	547.7	411.3	0.124	0.0032	0.0110
Corners	601.6	607.6	556.9	556.9	389.0	0.124	0.0030	0.0110

Note: Young's Modulus, E = 200 GPa

Table 7 Parameters for the stress-strain curves for the beams of the test structure

Floor	1		2		3		4	
Section	W18 × 46		W16 × 40		W16 × 31		W12 × 22	
	Expected*	Measured	Expected*	Measured	Expected*	Measured	Expected*	Measured
σ_{yf}	55.8	50.3	55.8	45.1	55.8	43.4	55.8	44.3
$b_f / 2t_f$	5.0	5.2	6.9	6.9	6.3	6.7	4.7	5.4
β_f	0.72	0.71	0.99	0.89	0.91	0.85	0.68	0.69
σ_{yw}	55.8	52.7	55.8	53.0	55.8	47.4	55.8	48.6
h / t_w	44.6	44.0	46.6	47.7	51.6	51.4	41.8	41.5
β_w	0.64	0.61	0.67	0.67	0.74	0.68	0.60	0.56
β	0.68	0.66	0.85	0.79	0.83	0.77	0.64	0.63
σ_m / σ_y	1.26	1.26	1.25	1.26	1.25	1.26	1.26	1.27
$\varepsilon_r / \varepsilon_y$	11,200	12,000	6,800	8,000	6,800	9,000	13,000	14,000

* According to Dexter *et al*. (2000)

Table 8 Test structure connection model properties

Floor	Rotational spring		Vertical spring	
	M_{sy} (kN-m)	K_θ (kN-m/rad)	V_{sy} (kN)	K_V (kN/mm)
4	415.8	68763	1090	1543
3	652.9	202661	1165	4994
2	757.6	294594	1059	14324
1	929.9	450311	1103	17417

Table 9 Panel zone model properties of the test structure

Floor	M_y (kN-m)	γ_y (rad)	M_p (kN-m)	γ_u (rad)
4	600.6	0.00234	1001.0	0.01012
3	774.6	0.00234	1291.2	0.01012
2	781.2	0.00230	1301.8	0.00995
1	881.1	0.00230	1468.6	0.00995
G	881.1	0.00230	1468.6	0.00995

developed by Varma *et al*. (2005).

The data defining the concrete and steel tube stress-strain curves for the CFT are presented in Tables 5-6, respectively. The number of fibers to discretize the cross section of a CFT of the test structure is similar to that shown in Fig. 5. The cross section of each WF beam was discretized using 5 fibers, as described previously. The parameters to define the stress-strain curves for the WF beams of the test frame are given in Table 7.

The properties of the connection and panel zone models are listed in Tables 8-9. These properties were calibrated to the measured force-displacement response at the ground level obtained during the low intensity earthquake tests (i.e., the frequently occurring earthquake, FOE) performed by Herrera *et al*. (2008). In addition, the loading beam segment between the two bays was modeled using elastic beam elements The elastic beam elements were pin connected to the test structure beams at mid-span. The loading beam model also emulated the restraint against axial shortening of the test structure beams imposed by the loading beams.

In the analytical model the gravity load on the test structure model was applied as concentrated loads acting at midspan on the beams, at the top node of the panel zones in the columns, and at the nodes of a lean-on column at each floor level, as shown in Fig. 9(b). The lean-on column was used to capture the P-Δ effects associated with the gravity load from the gravity frames. In Fig. 9(b) P_c is the weight of the test structure column at each story, $2P_g$ is the combined weight of the test structure beams, connections, and attached lateral loading apparatus at each floor, and P_{lc} is the gravity load applied to the lean-on column at each floor level, acting on one-half of the columns of the gravity load

Table 10 Gravity loads applied to test structure model

Floor	P_c (kN)	P_g (kN)	P_{Lc} (kN)
4	13	18	1036
3	22	27	1424
2	22	27	1424
1	22	27	1424
G	0	0	0

Table 11 Floor mass of test frame

Floor	Mass (kg)
4	106,000
3	146,000
2	146,000
1	146,000
G	0

Table 12 Experimental and analytical model initial elastic natural periods of the test structure

Mode	Initial Elastic Natural Period – T (sec)		
	Experimental	Analytical	Difference
1	1.211	1.139	-5.9%
2	0.369	0.395	7.0%
3	0.203	0.203	0.0%
4	0.148	0.128	-13.5%

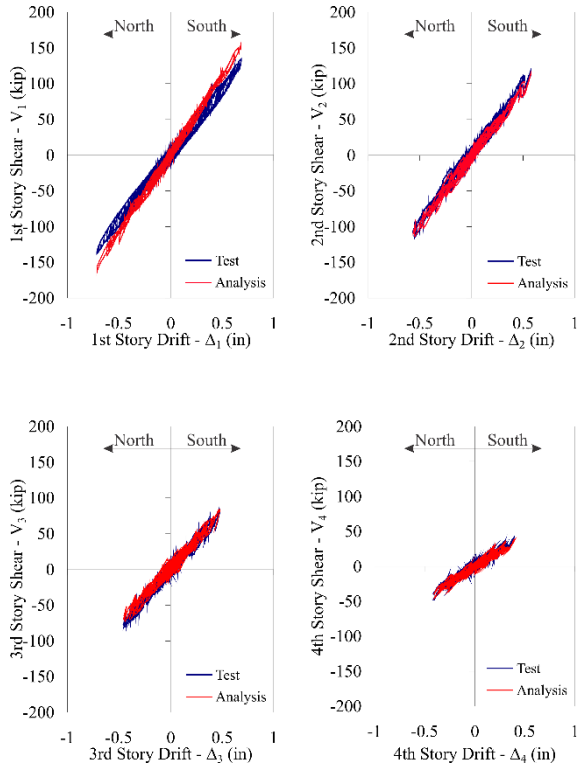

(a) Story shear-story drift response

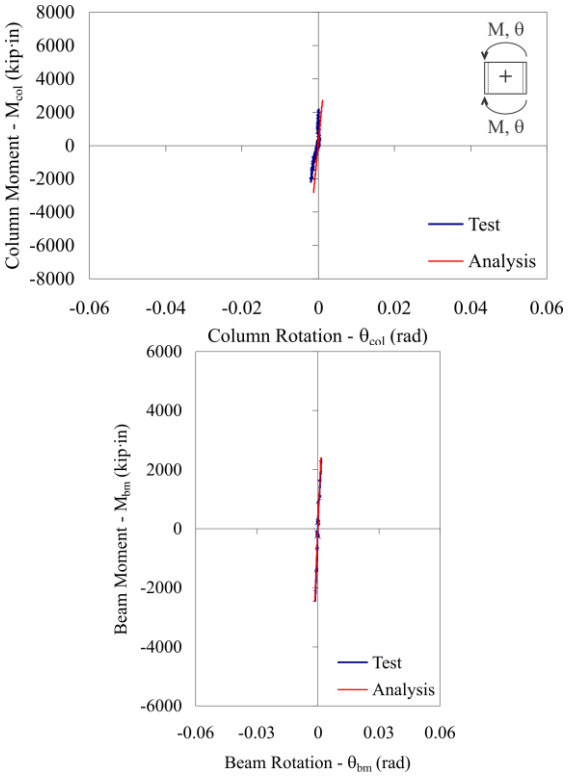

(b) 1st story middle column base and north end of north beam moment-rotation response

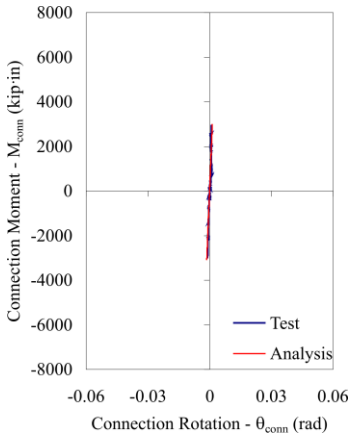

(c) 1st story north end of north beam connection moment-rotation response

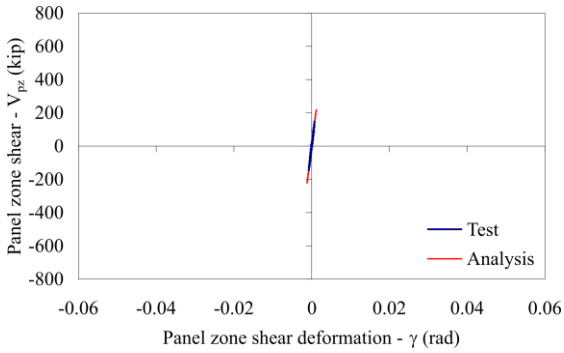

(d) 1st story middle panel zone force-deformation response

Fig. 10 Analytical vs. experimental response of CFT-MRF test structure; FOE test by Herrera *et al*. (2008)

system, tributary to the prototype frame and multiplied by the force scale factor. The gravity loads applied to the test structure model are given in Table 10.

The mass at each floor level was placed at the lean-on column, resulting in a lumped mass matrix. The mass of the test structure was based on the tributary floor of the CFT-MRF, and equal to the values shown in Table 11.

3.2 Modeling evaluation procedure

First, the test structure stiffness matrix and natural periods were determined from the analytical model and compared to the stiffness matrix and natural periods determined experimentally. In the calculation of the analytical stiffness matrix, the same procedure used for the experimental determination of these quantities was followed: a displacement of 2.5 mm was applied at each floor while keeping the other floors fixed, and the forces at each degree of freedom were recorded and divided by the displacement to obtain the associated column of the stiffness matrix. An eigenvalue analysis was then conducted to obtain the natural periods of the test structure model, using the analytical mass matrix assigned to the test structure (see Table 11).

Next, the complete set of tests was simulated using the test structure analytical model. This involved imposing the history of measured floor displacements from the test structure to the analytical model. The state of the structure

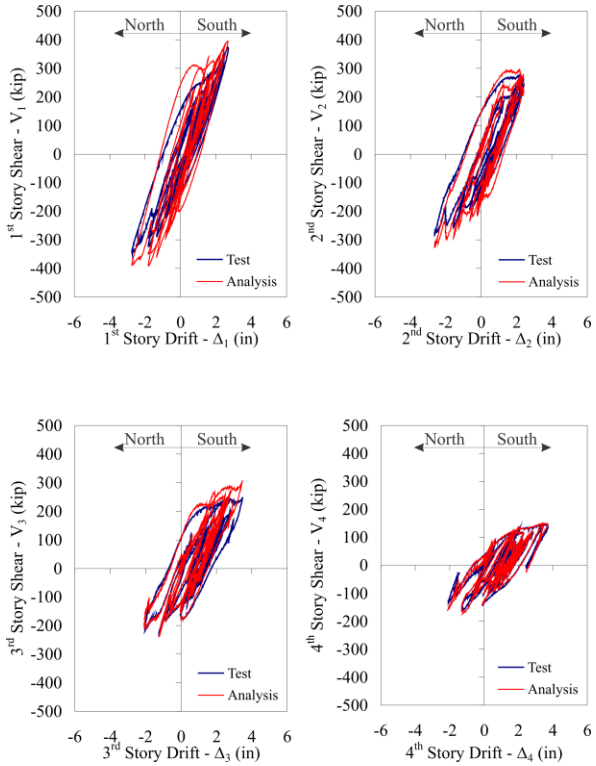

(a) Story shear-story drift response

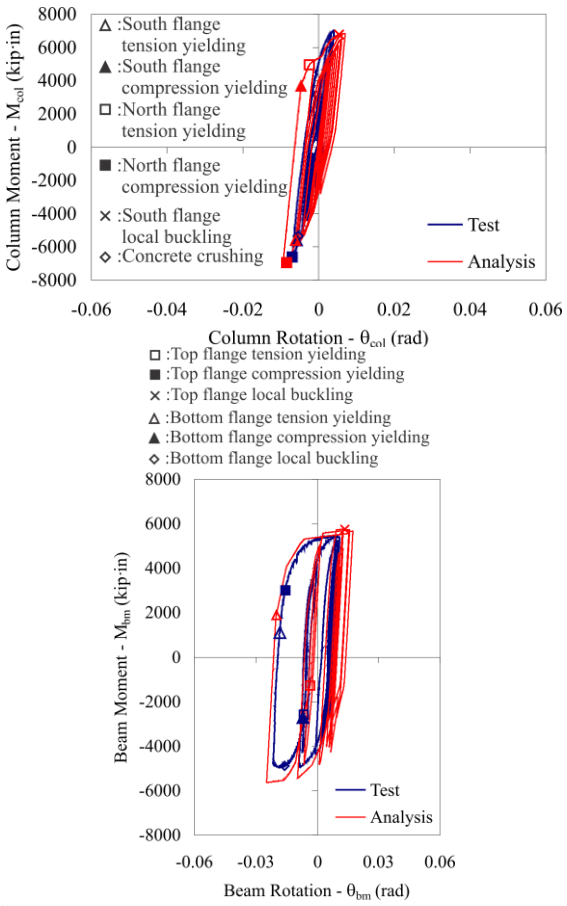

(b) 1st story middle column base and north end of north beam moment-rotation response

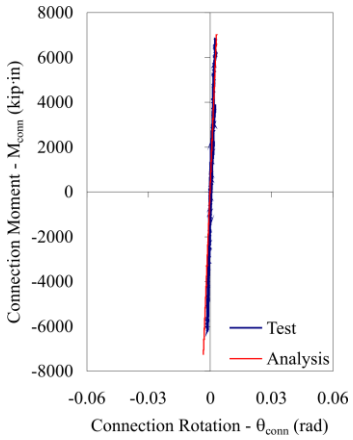

(c) 1st story north end of north beam connection moment-rotation response

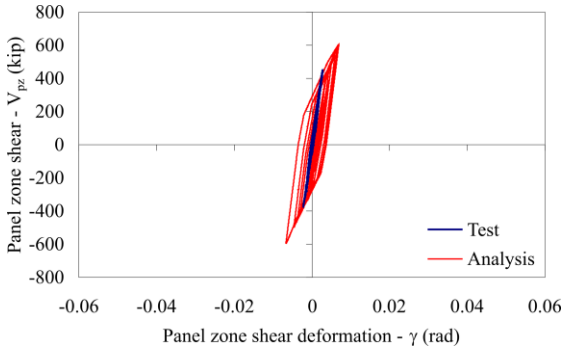

(d) 1st story middle panel zone force-deformation response

Fig. 11 Analytical vs. experimental response of CFT-MRF test structure; DBE test by Herrera *et al*. (2008)

was determined in terms of internal forces and story shears associated with the imposed displacements to the model, which was then compared to the experimental measured response of the test structure to evaluate the modeling procedure for CFT-MRFs. To account for some support motion that occurred in the test setup, measured displacement histories at the supports were applied to the test structure analytical model. For the sake of consistency and due to the loss of the south bay displacement data during the MCE test, only the north bay displacement histories were imposed at each floor, and the loading beam model was used to impose consistent displacements to the south bay. See Fig. 9(a) for the definition of the north and south directions. The measured displacements of the column pinned bases and the reaction points at the ground level were simultaneously imposed to have the same boundary conditions for the analytical model be the same as those of the test structure. The measured displacement histories from each test were sequentially imposed to the model, using as initial conditions those conditions at the

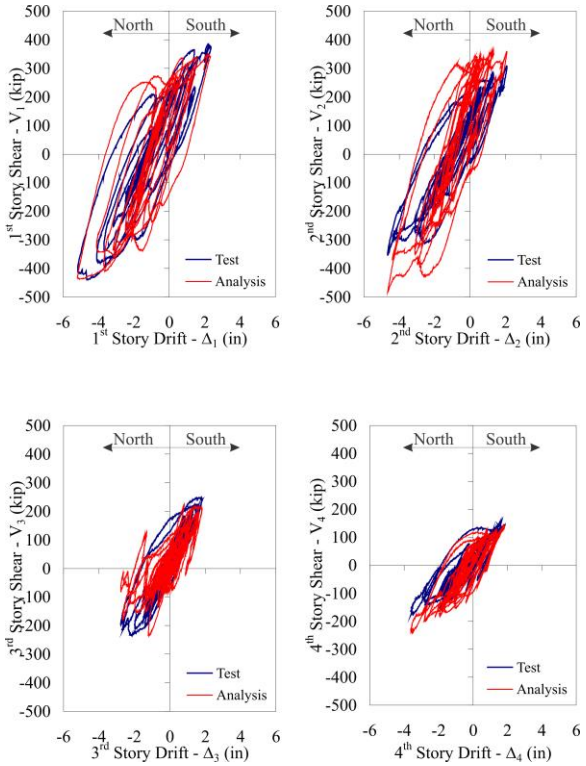

(a) Story shear-story drift response

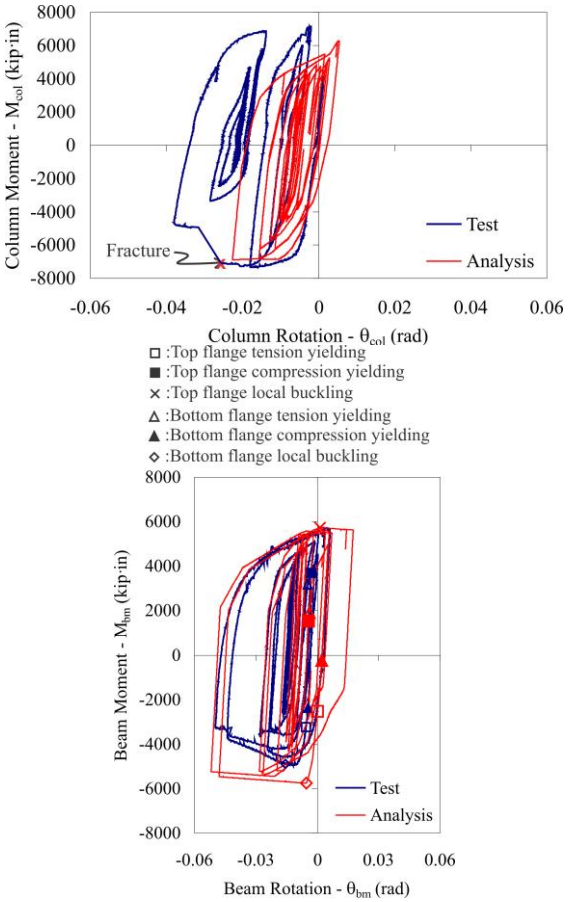

(b) 1st story middle column base and north end of north beam moment-rotation response

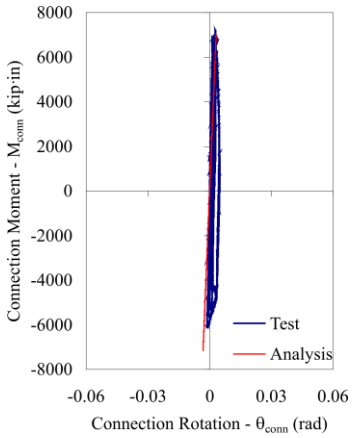

(c) 1st story north end of north beam connection moment-rotation response

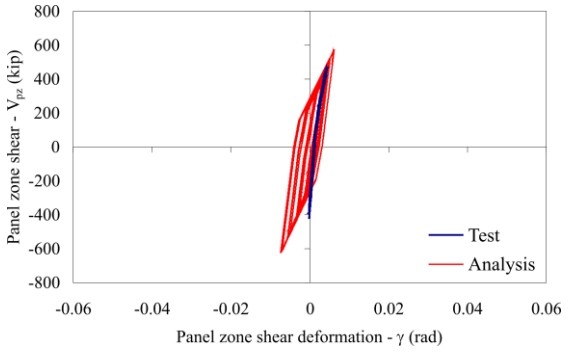

(d) 1st story middle panel zone force-deformation response

Fig. 12 Analytical vs. experimental response of CFT-MRF specimen. MCE test by Herrera *et al*. (2008)

final state of the prior analysis.

3.3 Comparison of test structure model and experimental results

The experimental and analytical natural periods are presented in Table 12. This table shows that the analytical model was stiffer than the actual test structure, as indicated by the shorter first mode period of the model with respect to the test structure.

Comparisons between the analytical predictions and experimental results are presented for tests representative of the FOE, DBE, and MCE earthquake hazard levels.

The comparison of the story shear-story drift response from the experiment and the analysis is shown in Fig. 10 for the FOE level test. Good agreement can be observed for all stories except the first, which exhibits a lower experimental stiffness (test) with respect to the stiffness predicted by the model (analysis). This result coincides with the difference found between the experimental and analytical first mode

periods. The stiffness of the columns, beams and connections at the 1st story is well predicted by the model, as well as the stiffness of the panel zones at this story, but the panel zone deformation is overestimated.

Fig. 11 shows the comparison between the experimental and analytical model results for the DBE level test. The analytical model adequately predicts the experimental story shear-story drift response (Fig. 11(a)). The experimental results for the 1st story exhibit a slightly lower stiffness than that predicted by the model, but the difference in maximum story shear between the experimental result and analytical prediction is smaller in the DBE test than in the FOE test. Good correlation between the analytical predictions and the experimental results is also observed in the member response. The response at the base of the first story interior CFT-MRF column is represented properly, however, differences in the maximum moments are observed in Fig. 11(b). This suggests that the difference in the 1st story stiffness observed between the analytical model and the experiments is due to flexibilities not captured by the model below the 1st story column bases (i.e., the columns below the ground level that are pinned-ended as shown at the base of the structure in Fig. 9). The moment-rotation response of the beams is reasonably reproduced by the analytical model, as shown in Fig 11(b). However, the occurrence of local buckling is not predicted properly. This discrepancy may be related to a shortcoming of the beam plastic hinge model, which was calibrated for beams in pure bending. The beams in the test structure and the model also are subjected to axial load from the lateral loading applied to the loading beams of the test structure.

The connection model reproduces reasonably well the behavior of the connections in the test structure (Fig. 11(c)). The forces and deformations of the panel zone are slightly over predicted, which indicates the need for improving the determination of the parameters that define the panel zone model response, e.g., elastic stiffness ($K_{\gamma,e}$), panel zone shear at the onset of inelastic behavior (V_y), inelastic stiffness ($K_{\gamma,i}$), and panel zone shear capacity (V_u).

The analysis of the test structure model subjected to the MCE test could not be carried out in its entirety with the original model due to lack of convergence during the analysis. The convergence problems were generated in the plastic hinge models for the 4th floor beams and the base of the 1st story columns, which occurred when most of the steel fibers of the cross section in these regions reached the post-buckling descending stress branch, causing the elements to have a negative stiffness. Therefore, the model was modified to obtain a converged solution. The modifications included the elimination of the descending branch for the web steel fibers of the column plastic hinge model and the use of an elastic (instead of an elastic perfectly plastic) web fiber for the middle fiber of the beam plastic hinge models at the 4th floor only.

The comparison of the story shear-story drift response from the experiment and the analysis is shown in Fig. 12(a). Good agreement between the experimental and analytical results is observed for the 1st story, while the 2nd, 3rd, and 4th story analytical responses exhibit greater differences when the drift is in the north direction compared to the south direction.

Fig. 12(b) presents the moment-rotation response at the base of the 1st story middle (i.e., interior) column and at the north end of the 1st story north beam. The model predicts reasonably well the capacity of the CFT columns, but the rotation is underestimated after a fracture occurs in the steel tube during the experiment, because fracture is not modeled. The maximum beam moments predicted by the model are larger than the experimental values. Yielding of the beam flanges is adequately predicted, but local buckling was not reproduced accurately. The model did not capture the strength degradation at the north end of the 1st floor north beam, which was caused by extensive local buckling of the bottom beam flange and the web in the plastic hinge region.

The connection response (Fig. 12(c)) remains nearly elastic and is well reproduced by the model. The panel zone experimental shear force-shear deformation response and the analytical results are shown in Fig. 12(d). The response does not differ significantly from the response to the DBE, where the model predicts yielding of the middle panel zone which is not observed in the experimental results.

In summary, the agreement between the experimental and analytical results for the MCE level test is not as good as for the DBE level test, including the 2nd and 3rd story shear-story drift responses. The causes of this can be inferred by looking at the component response (i.e., CFT columns, WF beams, connections, and panel zones) and the modifications introduced to the model to achieve convergence in the test structure model for MCE test. Local buckling was not observed in the CFT columns during the experiments, and therefore the suppression of local buckling of the web fibers in the model did not have a significant effect on the agreement between the experimental and analytical results. However, the fracture generated in the middle column, which was not considered in the model, did have an effect, as seen in Fig. 12(b). The model represents the local buckling, but it does not accurately capture the strength deterioration. The strength of the panel zone is underpredicted by the model.

4. Conclusions

A summary of modelling of the components of a CFT-MRF based on experimental research, along with the development of an analytical model for a CFT-MRF system under seismic loading were presented. This model accounts for nonlinearities due to WF beam yielding and local buckling, CFT column concrete cracking and crushing, CFT steel tube yielding and local buckling, split-tee connection yielding, and panel zone concrete cracking and steel yielding.

An analytical model of a large scale CFT-MRF test structure was used to create analytical predictions of the experimental results for the test structure under simulated seismic loading, with the objective of validating the modelling procedure. The displacements of the test structure measured during a sequence of experiments, including the floor displacements and the displacements at

the supports were imposed on the analytical model of the test structure sequentially. The analytical predictions from the model were compared with the measured results for the test structure during the experiments.

Good agreement was found between the experimental results and analytical predictions in terms of story shear-story drift response. The first story was more flexible than predicted by the model. Locally, the model reproduced reasonably the response of the CFT columns, WF beams, and connections. The stiffness of the panel zones was well predicted by the model, but the capacity of panel zones and connections could not be compared because these elements remained elastic and never reached their capacity during the experiments. The capacity of WF beams and CFT columns was reasonably reproduced by the model. There were, however, some difficulties with the analytical model, due to element convergence issues, when the effects of extensive local buckling led to a significant deterioration in member capacity.

The analytical model provides reasonable estimates of the response of the frame only up to the initiation of a fracture in the first story middle column. This limit state was not included in the model and the sudden change in force and displacement that accompanied the fracture was not included in the model.

Based on the ability of the analytical model to predict the relevant limit states that develop in a CFT-MRF under seismic loading, the modelling procedure presented in this paper is deemed suitable and recommended to be used for conducting nonlinear analyses of CFT-MRF systems, particularly where the global response under seismic loading, such as story shear and drift, are of interest.

Acknowledgments

The research reported herein was supported by the National Science Foundation (Grant. No. CMS-9905870) and by a grant from the Pennsylvania Department of Community and Economic Development through the Pennsylvania Infrastructure Technology Alliance. The opinions expressed in this paper are those of the authors and do not necessarily reflect the views of the sponsors.

References

AISC (2005), *ANSI/AISC 341-05: Seismic Provisions for Structural Steel Buildings*, American Institute of Steel Construction, Chicago, IL, USA.

AISC (2017), *Steel Construction Manual* (15th Edition), American Institute of Steel Construction, Chicago, IL, USA.

COMSOL Inc. (2013), *COMSOL - Software for Multiphysics Simulation*, COMSOL Group, Stockholm, Sweden. http://www.comsol.com

Dexter, R., Graeser, M., Saari, W., Pascoe, C., Gardner, C. and Galambos, T. (2000), *Structural Shape Material Property Survey*, Final Report, prepared for the Structural Shapes Producers Council by the University of Minnesota, Department of Civil Engineering, Minneapolis, MN, USA.

FEMA (2003), *NEHRP Recommended Provisions for New Buildings and Other Structures*. *Part 1-Provisions*, Rep. No. FEMA 450, Washington, DC, USA.

Fujimoto, T., Nishiyama, I., Mukai, A. and Baba, T. (1996), "Test results of concrete filled steel tubular beam-columns", *Proceedings of the Third US-Japan Joint Technical Coordinating Committee on Composite and Hybrid Structures*, Hong Kong, China.

Hajjar, J.F., Molodan, A. and Schiller, P.H. (1998a), "A distributed plasticity model for cyclic analysis of concrete-filled steel tube beam-columns and composite frames", *Eng. Struct*., **20**(4-6), 398-412. https://doi.org/10.1016/S0141-0296(97)00020-5.

Hajjar, J.F., Schiller, P.H. and Molodan, A. (1998b), "A distributed plasticity model for concrete-filled steel tube beam-columns with interlayer slip", *Eng. Struct*., **20**(8), 663-676. https://doi.org/10.1016/S0141-0296(97)00107-7.

Herrera, R., Ricles, J.M. and Sause, R. (2008), "Seismic performance evaluation of a large-scale composite MRF using pseudodynamic testing", *J. Struct. Eng. ASCE*, **134**(2), 279-288. https://doi.org/10.1061/(ASCE)0733-9445(2008)134:2(279).

Inai, E. and Sakino, K. (1996), "Simulation of flexural behavior of square concrete filled steel tubular columns", *Proceedings of the Third US-Japan Joint Technical Coordinating Committee on Composite and Hybrid Structures*, Hong Kong, China.

Kanatani, H., Tabuchi, M., Kamba, T., Hsiaolien, J. and Ishikawa, M. (1987), "A study on concrete filled RHS column to H-beam connections fabricated with HT bolts in rigid frames," *Proceedings of the First Composite Construction in Steel and Concrete Conference*, Engineering Foundation, Henniker, NH, USA.

Kim, T., Whittaker, A.S., Gilani, A.S.J., Bertero, V.V. and Takhirov, S.M. (2000), *Cover-Plate and Flange-Plate Reinforced Steel Moment Resisting Connections*, Report No. PEER 2000/07, Pacific Earthquake Engineering Research Center, University of California at Berkeley, Berkeley, CA, USA.

Koester, B. (2000), *Panel Zone Behavior of Moment Connections Between Rectangular Concrete-Filled Steel Tubes and Wide Flange Beams*, Ph.D. Dissertation, Dept. of Civil and Environmental Engineering, University of Texas, Austin, TX, USA.

Mehanny, S.S.F. and Deierlein G.G. (2001), "Seismic damage and collapse assessment of composite moment frames", *J. Struct. Eng. ASCE*, **127**(9), 1045-1053. https://doi.org/10.1061/(ASCE)0733-9445(2001)127:9(1045).

Muhummud, T. (2004), *Seismic Behavior and Design of Composite SMRFs with Concrete Filled Steel Tubular Columns and Steel Wide Flange Beams*, Ph.D. Dissertation, Dept. of Civil and Environmental Engineering, Lehigh University, Bethlehem, PA, USA.

Peng, S.W., Ricles, J.M. and Lu, L.W. (2001), *Seismic Resistant Connections for Concrete Filled Column-to-WF Beam Moment Resisting Frames*, ATLSS Report No. 01-08, Lehigh University, Bethlehem, PA, USA.

Prakash, V., Powell, G.H. and Campbell, S. (1993), *DRAIN-2DX Base Program Description and User Guide*, Report No. UCB/SEMM-93/17&18, Department of Civil Engineering, University of California, Berkeley, CA, USA.

Ricles, J.M., Mao, C., Lu, L. and Fisher, J. (2002), "Inelastic cyclic testing of welded unreinforced moment connections", *J. Struct. Eng. ASCE*, **128**(4), 429-440. https://doi.org/10.1061/(ASCE)0733-9445(2002)128:4(429).

Ricles, J.M., Peng, S.W. and Lu, L.W. (2004), "Seismic behavior of composite concrete filled steel tube column-wide flange beam moment connections", *J. Struct. Eng. ASCE*, **130**(2), 223-232. https://doi.org/10.1061/(ASCE)0733-9445(2004)130:2(223).

SAC (1997), *Connection Test Summaries*, Report No. FEMA-289 or SAC-96-02, SAC Joint Venture, CA, USA.

Swanson, J.A. and Leon, R. (2001). "Stiffness modeling of bolted T-stub connection components", *J. Struct. Eng. ASCE*, **127**(5), 498-505. https://doi.org/10.1061/(ASCE)0733-9445(2001)127:5(498).

Tomii, M. and Sakino, K. (1979), "Experiment studies on the ultimate moment of concrete filled square steel tubular beam-columns", *Trans. Archit. Inst. of Japan*, **275**, 55-63.

Varma, A.H., Ricles, J.M., Sause, R. and Lu, L.W. (2004), "Seismic behavior and design of high strength square concrete-filled steel tube beam-columns", *J. Struct. Eng. ASCE*, **130**(2), 169-179. https://doi.org/10.1061/(ASCE)0733-9445(2004)130:2(169).

Varma, A.H., Ricles, J.M., Sause, R. and Lu, L.W. (2002), "Experimental Behavior of High Strength Square CFT Beam-Columns", *J. Struct. Eng. ASCE*, **128**(3), 309-318. https://doi.org/10.1061/(ASCE)0733-9445(2002)128:3(309).

Varma, A.H., Sause, R., Ricles, J.M. and Li, Q. (2005), "Development and validation of fiber model for high-strength square concrete-filled steel tube beam-columns", *ACI Struct. J.*, **102**(1), 73-84. https://doi.org/10.14359/13532.

Zhang, W. and Shahrooz, B.M. (1997), *Analytical and Experimental Studies into Behavior of Concrete-Filled Tubular Columns*, Report No. UC-CII 97/01, Cincinnati Infrastructure Institute, University of Cincinnati, Cincinnati, OH, USA.

CC